Ab initio potentials of F + Li-2 accessible at ultracold temperatures

Ab initio potentials of F + Li_2 accessible at ultracold temperatures

K. W. A. Wright and Ian C. Lane*

Innovative Molecular Materials Group, School of Chemistry and Chemical Engineering, Queen's University of Belfast, Stranmillis Road, Belfast BT9 5AG, UK

(Received 30 March 2010; revised manuscript received 6 July 2010; published 29 September 2010)

Ab initio calculations for the strongly exoergic Li_2 + F harpoon reaction are presented using density-functional theory, complete active space self-consistent field, and multireference configuration interaction methods to argue that this reaction would be an ideal candidate for investigation with ultracold molecules. The lowest six states are calculated with the aug-correlation-consistent polarized valence triple-zeta basis set and at least two can be accessed by a ground rovibronic Li_2 molecule with zero collision energy at all reaction geometries. The large reactive cross section (characteristic of harpoon reactions) and chemiluminescent products are additional attractive features of these reactions.

DOI: 10.1103/PhysRevA.82.032715 PACS number(s): 34.50.Lf, 31.15.vq, 34.20.Gj

I. INTRODUCTION

In 1982, a beam of alkali-metal atoms was successfully decelerated by 40% using a counterpropagating laser beam [1]. The subsequent success of laser cooling in producing slow kinetically cold atoms and its extension to atom trapping has had a revolutionary effect on atomic physics and, since the creation of the dilute Bose-Einstein condensate (BEC) a decade ago [2], a perhaps even greater influence on condensed matter physics. Already ultracold molecules can be prepared in a selected quantum state either close to the dissociation limit [3] (magnetic Feshbach resonances) or in the ground vibrational state [4] (STIRAP). All this recent work has marked a significant shift in the attitude to quantum scattering resonances: No longer just intriguing phenomena to be measured and perhaps catalogued, they are now used as a tool for the manipulation of matter. The production of quantum-state-selected ultracold molecules [5] is also the realization of a dream for physical chemists for it signals the end of the ubiquity of the Boltzmann distribution. Such molecules will no doubt be harnessed into new experiments on quantum state dynamics and the question now is what types of chemical processes can be studied with such unique reagents. At first ultracold chemistry seems a rather unlikely prospect because most reactions have barriers on the potential energy surface that would seem to exclude reactive collisions with near-zero kinetic energies. These objections can be refuted in three ways: (1) Molecules formed in ultracold gases can be prepared with an enormous amount of internal energy that can be used to overcome reaction barriers, (2) the ultracold temperatures facilitate quantum mechanical tunneling through reaction barriers, and (3) there are chemical reactions that do not have reaction barriers. A popular class of barrierless reactions are those adopting the so-called harpoon mechanism, studied extensively half a century ago in chemistry's own "alkali age" [6].

Perhaps surprisingly, the reaction of alkali-metal dimers and halogen atoms is possibly one of the oldest in the canon of reaction dynamics, with ground-breaking experiments performed in sodium-halogen flames by Michael Polanyi in the 1920s [7]. Strong luminescence is observed from electronically excited alkali-metal atoms formed via chemical reaction in the flame. As Struve *et al.* were to demonstrate conclusively some fifty years later, a significant step [8] in the production of chemiluminescent alkali-metal atoms is the three-atom collision

$$M_2 + X \rightarrow MX + M^*.$$

Such a reaction has a total cross section larger than the predicted collision rate, a discrepancy eloquently explained by Polanyi as an electron "harpoon" that reels in the electron acceptor from long range. The harpoon mechanism is a remarkably simple model to explain a variety of chemical reactions that possess very large collision cross sections. A significant early work was that of Magee [9], who formalized this model into nonadiabatic crossings between (attractive) ionic and covalent potentials. The ionic potential can be described quite accurately by a Rittner [10] potential function, which modifies the basic Coulomb potential with additional polarization terms:

$$\phi = -\frac{e^2}{R} - \frac{e^2(\alpha_1 + \alpha_2)}{2R^4} - \frac{2e^2\alpha_1\alpha_2}{R^7}.$$

However, this model tells us nothing about the behavior of the covalent potential as a function of R, the distance between the centers of mass of the two reactants. That must be determined by other means.

Barrierless reactions are attractive candidates for the study of chemical dynamics at virtually zero collision energies (s-wave scattering). Strong evidence for an exchange reaction between Cs_2 dimers and Cs atoms has been presented by Grimm and co-workers [11] to explain an increase in atom loss from an ultracold gas of Cs atoms when a magnetic field is applied, and recently Ye and co-workers have shown that a pair of ground-state KRb molecules can react [12] at 150 nK to produce molecular products K_2 + Rb_2 (with an energy release of just 10 cm^{-1}). At this time no detection of the product molecules has been reported. A recent set of Møller-Plesset second-order perturbation theory (MP2) and coupled-cluster with single and double perturbative triple excitations [CCSD(T)] calculations by Chandra and co-workers [13] report the exoergicity of the reaction Li_2 + F → LiF + Li to be 41 501 cm^{-1} (MP2) or 39 043.7 cm^{-1} [CCSD(T)].

*Corresponding author: i.lane@qub.ac.uk

Such an enormous exoergicity simplifies the detection of reaction products: Indeed, in the most comprehensive study of halogen reactions with alkali-metal dimers by Struve and co-workers, chemiluminescence [14] from the excited atomic products was used to assign the alkali electronic states following single atom-molecule collisions in a crossed-beam chamber. This solves a significant drawback in using cold and trapped reagents for reaction dynamics experiments where the trapping potential will inevitably influence the reaction products formed. By observing the fluorescence, the nascent population distributions of the reaction products are observed.

In this paper, *ab initio* calculations are performed using density functional theory (DFT), state-averaged complete active space self-consistent field (SA-CASSCF), and multireference configuration interaction (MRCI) methods on the model electron transfer system $Li_2 + F$. The details of these calculations are outlined in Sec. II. The results will concentrate on the entrance (Sec. III) and exit (Sec. IV) channel potentials, the latter corresponding to lithium atom products up to and including Li($3p$). The calculations demonstrate the existence of mixed ionic-covalent character in the exit-channel $^2\Sigma^+$ states corresponding to each asymptotic limit. This is indicative of multiple crossings between an ionic surface which is bound and forms the global minimum and a series of repulsive covalent surfaces. The net result is a series of bound adiabatic $^2\Sigma^+$ potentials with the crossing distance between ionic and covalent surfaces, and therefore the potential minima, increasing with the energy of the lithium atom product. As surface hopping is maximized close to these crossing points, the surfaces suggest it may be possible to exploit the long-range character of the Li_2 vibrational wave function close to the dissociation limit (typical of Feshbach resonances) to select the electronic states of the lithium atom products (Sec. V).

II. *AB INITIO* METHODS

Since the broad features of these reactions has been successfully analyzed using the harpoon model there has been less attention paid to calculating accurate potential energy surfaces than to rival benchmark systems such as $H_2 + H$ and $H_2 + F$. Some thirty years after Magee's initial work, Balint-Kurti [15] calculated potential curves for the $Li_2 + F \rightarrow LiF + Li$ reaction using the orthogonalized Moffitt (OM) method. This is probably still the most accurate work available, but even this did not study the region around the ground-state harpoon radius. Note that there are strong similarities [16] between the ground-state surface of Li_2F and that of Li_2H, which is also an ionic complex.

In the absence of spin-orbit coupling, the approach of a ground-state halogen atom to an alkali-metal dimer will take place along three covalent potentials ($2\,^2A'$ and $1\,^2A''$ in C_s symmetry), two of which are degenerate ($^2\Pi$) in the collinear reaction geometry. The two $^2A'$ states will also be crossed by an ionic $^2A'$ potential that forms the global potential minimum. This harpoon mechanism is disfavored in most bimolecular systems because of the high ionization energy of the donor (since most atoms and molecules have an ionization potential in excess of 6 eV) and/or the small electron affinity of the acceptor molecule (see Table I for a list of parameters relevant to this study). This means that any crossing between the covalent and ionic potentials will take place at very short bond distances. The $Li_2 + F$ reaction, however, benefits from the low ionization energy of Li_2 and the exceptionally high electron affinity of the fluorine atom. The ionic potential correlating to the $Li_2^+(1\,^2\Sigma_g^+) + F^-(^1S_0)$ asymptote needs to fall by just 14 062 cm^{-1} in order to cross the ground-state covalent potential [which at long range corresponds to the ground-state reagents Li_2 $(1\,^1\Sigma_g^+)$ + F (^2P)]. This means that the steep inner wall of the covalent potential lies well within the ionic-potential crossing point. However, in order for the ground-state potential to be truly barrierless the covalent potential must either fall or remain flat from the asymptote to the crossing point. This issue is one of the main motivations for this study.

TABLE I. Atomic and molecular parameters relevant to the $Li_2 + F$ reaction.

Physical parameter	Value (experimental unless stated)
^{7}Li ionization energy [17]	43 487.159 cm^{-1}
$^7Li_2$ ionization energy [18]	41 494.6 cm^{-1}
^{19}F electron affinity [19]	27 432.446 cm^{-1}
α(Li) [20]	$165a_0^3$ (theory)
$\alpha(Li_2^+)$ [21]	$63a_0^3$ (theory)
$\alpha(F^-)$ [22]	$\sim 15a_0^3$ (theory)

The majority of our calculations were conducted using triple-zeta quality basis sets such as aug-cc-pVTZ [23] (here referred to as AVTZ). The work by Varandas [24] on LiF has shown that this quality of basis set can achieve an accuracy within 1% of the complete basis set (CBS) limit. The simplest calculations performed used DFT and a variety of exchange functionals in an attempt to model the entrance and exit channels of the ground potential energy surface and to determine the minimum energy geometry of the $M_2 + X$ reactions $Li_2 + [F, Cl, Br]$ and $F + [Na_2, K_2]$. The SA-CASSCF method was used to calculate the correct configurations present in each state's electronic wave function. This method was chosen because of the inherently multisurface nature of the harpoon reaction. Finally, the effect of dynamical electron correlation was determined by employing MRCI calculations using the SA-CASSCF wave functions as input. The Davidson correction [25] was applied to the MRCI results (MRCI + Q).

The calculations were performed using the FIREFLY software package [27] (which is a free *ab initio* program) on a LINUX cluster at Queen's University, typically using Core2 Duo or Quad processors, 2–8 Gbytes of RAM, and 320-Gbyte to 1-Tbyte hard drives. In a three-atom system, the Jacobi system uses the bond length of the diatomic, the distance between the diatomic center of mass and the third atom, and the angle between these two vectors θ. The Jacobi coordinate system was used to describe both the entrance and exit channels and consequently the coordinate system changes from reactant to product side: For instance, at the equilibrium geometry of the Li_2F complex calculated (with bond lengths of 1.697 Å) by Koput [28] $\theta_{bond} = 101^\circ$, $\theta_{entrance} = 90^\circ$, and $\theta_{exit} \approx 66^\circ$.

III. ENTRANCE-CHANNEL ELECTRONIC STATES

DFT calculations were performed on the reactions of Li_2 with a variety of halogens and on the reactions of F atoms with the first three homonuclear alkali-metal dimers. In each calculation, the diatomic bond length was held at its equilibrium bond length and the distance to the halogen atom varied while maintaining a collinear geometry (Fig. 1). There is a smooth approach to the asymptotic energies in all these calculations with no indication of a harpoon crossing point, suggesting that DFT methods are not ideal for the study of electron-transfer reactions of this particular kind.

The location of the harpoon radius on the potential energy surface is a critical consideration in this work because we wish to demonstrate that reagents with only zero-point energy (no collision energy) can react. Therefore a number of *ab initio* techniques were employed and their accuracy was determined by how closely they could match the harpoon radius of the simple Rittner model. To predict the harpoon radius in the entrance channel as a function of the Li_2 internuclear distance, the vertical ionization energy of the Li_2 molecular is required at each internuclear separation of the dimer. Such information can be found from *ab initio* calculations and the high-quality (an enhanced V5Z basis set equivalent, configuration interaction (CI) calculation) Li_2 and Li_2^+ potentials for the ground states of both species calculated by Sienkiewicz [29,30] and co-workers were used.

Calculations performed at both SA-CASSCF and MRCI + Q level confirm that the Li_2 + F reaction can proceed via a barrierless reaction pathway. In Fig. 2 SA-CASSCF calculations with a variety of basis sets at the Li_2 equilibrium bond length reveals that the lowest three bound states are

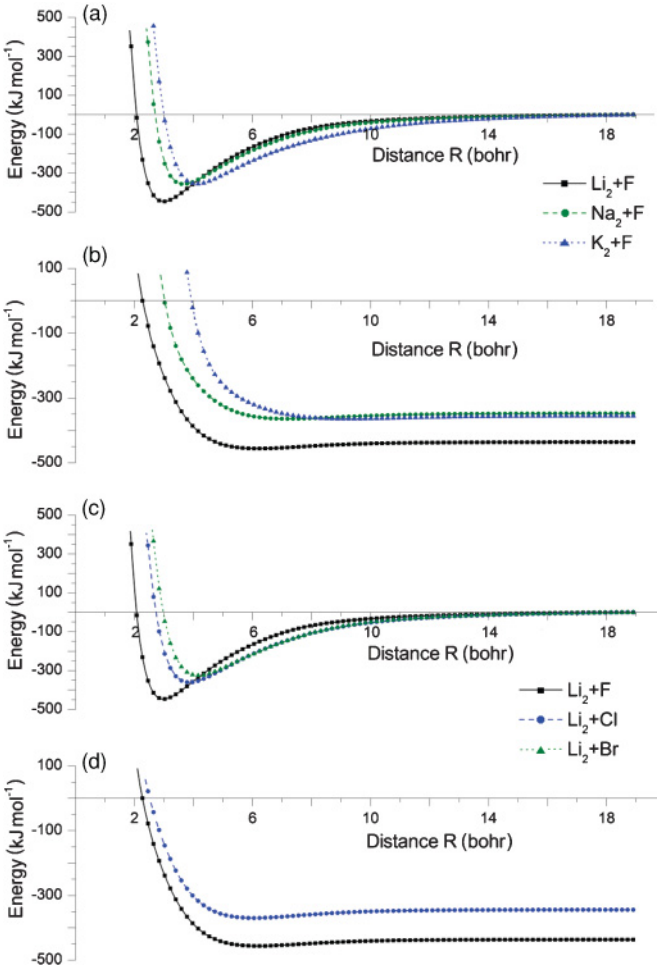

FIG. 1. (Color online) The entrance (a) and exit (b) channels of the M_2 + F series of reactions and (c) the entrance and (d) the exit for the Li_2 + X series of reactions, where M denotes an alkali-metal atom and X a halogen. Potentials are calculated by DFT using the 6-311++G(3df,3pd) basis sets and the MPW1K functional [26].

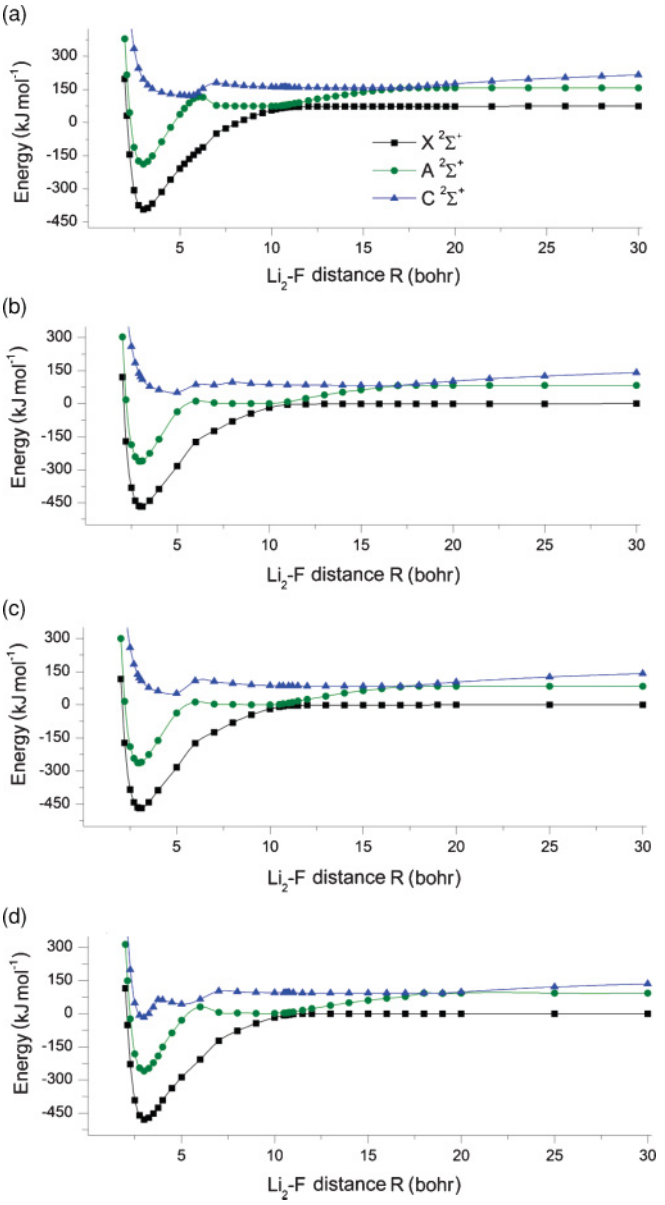

FIG. 2. (Color online) Li_2 + F entrance-channel potentials for the lowest three $^2\Sigma^+$ states calculated at the SA-CASSCF level with basis sets (a) VTZ (AVTZ); (b) AVTZ (AVTZ); (c) VQZ (AVQZ); and (d) a modified aug-6-311G (aug-6-311G) basis set, referring to the lithium (fluorine) atom. The lowest asymptote corresponds to the reagents Li_2 ($X\,^1\Sigma_g^+$) + F(^2P), the highest corresponds to the ionic species Li_2^+($X\,^2\Sigma_g^+$) + F^-(^2P), and the intermediate energy limit is Li_2 ($a\,^3\Sigma_u^+$) + F(^2P).

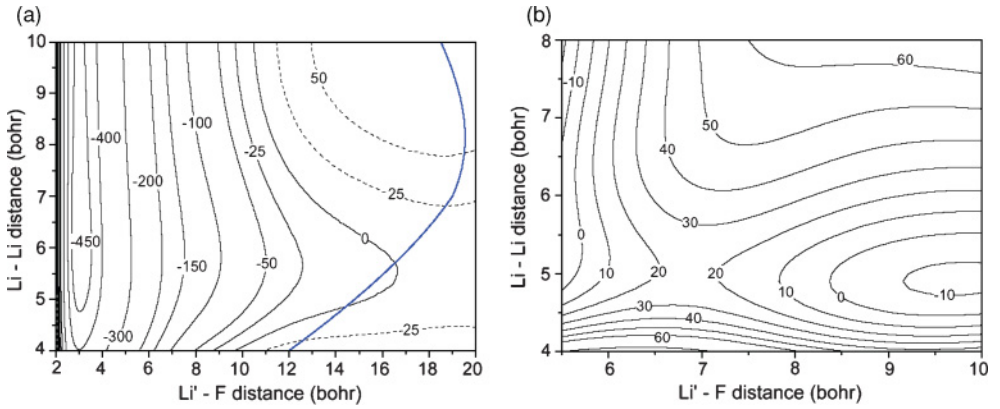

FIG. 3. (Color online) $Li_2 + F$ entrance-channel potentials in the collinear geometry as a function of both Jacobi separations. The potential energy surfaces were determined at the MRCI + Q level including two $^2\Sigma^+$ states based on a three-state SA-CASSCF calculation. (a) The ground-state potential: The surface has no barrier. The blue curve is the harpoon radius of the outer crossing point. (b) The $A\,^2\Sigma^+$ state which possesses a small barrier in the collinear geometry that will inhibit ultracold collisions on this surface. Note in both panels that the fluorine distance is measured from the closest lithium atom, not the center of mass.

accessible to ground electronic state reagents. The basis sets are VTZ(Li) and AVTZ(F) (panel a), AVTZ and AVTZ (panel b), VQZ and AVQZ (panel c), and a heavily modified aug-6-311 G basis set with additional diffuse functions similar to one adopted by Truhlar and co-workers in a calculation on the reaction Li + HF [31]. It is clear from Fig. 2 that the basis set chosen did not greatly affect the location of the outer crossing point (the outer harpoon radius). The results did show, however, some sensitivity to the number of states included in the SA-CASSCF calculation. The outer crossing point is too short according to the basic Rittner model (at a dimer separation of 6 bohr, the estimated harpoon distance H_R is 17.1 bohr) and is a well-documented problem with the SA-CASSCF method, which is further compounded when additional electronic states are added to the calculation (e.g., with a three-state SA-CASSCF, $H_R = 11.2$ bohr). A two-state SA-CASSCF calculation predicts a harpoon radius very close to the expected value for Li_2 at short bond lengths ($H_R = 15.8$ bohr) but such a limited number of states cannot be used at extended dimer bond lengths where both the $X\,^1\Sigma_g^+$ and $a\,^3\Sigma_u^+$ states of the dimer lie in close proximity to the ionic potential. Conducting a two-state MRCI calculation based on the three-state SA-CASSCF wave functions found for Fig. 1(b) increased the harpoon radius closer to the expected value ($H_R = 17.5$ bohr) and should be a more robust calculation.

In addition to the ground state, attention was focused on those excited states that may be accessible with zero-collision-energy reagents. This time there are stronger variations with basis set than before though a number of general features are apparent. The $A\,^2\Sigma^+$ state features a very long range crossing between the covalent $Li_2(a\,^3\Sigma_u^+) + F(^2P)$ asymptote and the ionic state, before becoming the upper state of the previous ionic-covalent interaction. The potential is then essentially the covalent $Li_2\,(a\,^3\Sigma_u^+) + F(^2P)$ surface until it is crossed at short range by a new, ionic surface. This surface is formed by the Coulomb interaction between ionic fragments $Li_2^+(1\,^2\Sigma_u^+) + F^-(^1S)$. However, the close approach required by the ions to facilitate the harpoon interaction (due to the internal excitation energy of the Li_2^+ ion) results in the crossing taking place on the repulsive wall of the covalent surface. This forms a barrier on the $A\,^2\Sigma^+$ surface, which may prevent collisions at low velocity from accessing this crossing region. The height of this barrier seems to be strongly basis set dependent and ranges from 1250 to 3340 cm^{-1} (15 to 40 kJ mol^{-1}).

Also displaying strong basis set sensitivity is the final $3\,^2\Sigma^+$ surface, which again features crossings involving the two ionic surfaces essential to the previous $A\,^2\Sigma^+$ state. All the basis sets broadly agree on the location of the outer crossing points and that there is a barrier that formed by the $Li_2^+(1\,^2\Sigma_u^+) + F^-(^1S)$ ionic surface and the $Li_2(a\,^3\Sigma_u^+) + F(^2P)$ covalent surface. However, the basis set containing the most diffuse atomic basis functions also predicts a third crossing with another ionic state close to the ground equilibrium bond length. As before this must correspond to an excited state of the Li_2^+ cation and the most likely candidate is the $2\,^2\Sigma_g^+$ state. However, attempts to augment both the AVTZ and AVQZ basis sets with similar diffuse functions failed to reproduce this crossing and its existence is still under investigation. Note that both the $1\,^2\Sigma_u^+$ and $2\,^2\Sigma_g^+$ states of Li_2^+ are bound but with equilibrium bond lengths (9.911 and 6.741 Å, respectively) much greater than that of the ground state (3.095 Å [32]). In fact both states are repulsive at the ground-state equilibrium bond length and lie above their respective atomic asymptotes.

The remaining calculations discussed in this section all used the AVTZ basis set on both lithium and fluorine. To explore the long-range ionic-covalent interaction further, three-state MRCI calculations were performed on the lowest $^2\Sigma^+$ states for the collinear reaction geometry as a function of the other two entrance-channel Jacobi coordinates. The resulting surfaces are shown in Fig. 3 and are based on nearly 600 *ab initio* points and include the Davidson correction. The ground potential has no barrier and a steep fall in energy with a small energy minimum. In contrast, the excited-state potential clearly has a barrier that will prevent reactions at ultralow collision energies. Also indicated on the ground potential energy surface is the crossing seam (harpoon seam) between the two surfaces at long range (blue curve online). In order to ensure that this harpoon seam was correct at the exit asymptote (where the distance is determined by the ionization energy of

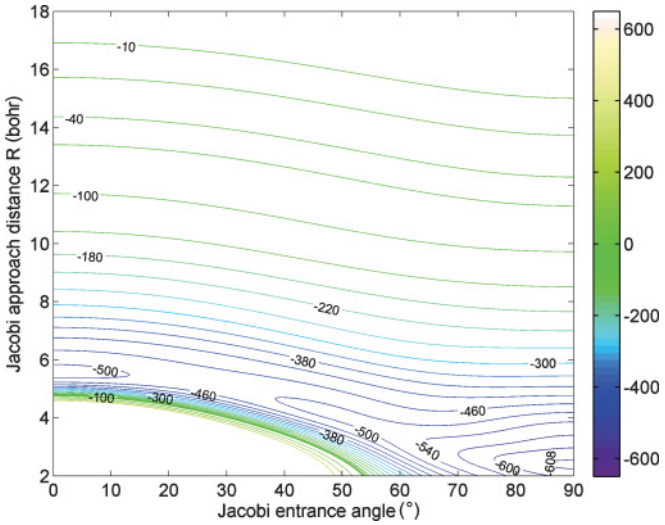

FIG. 4. (Color online) Li_2 + F entrance-channel $X\,^2A'$ (C_s symmetry) MRCI + Q potential as a function of incident Jacobi angle and the distance between the center of mass of the dimer (with separation held at 5 bohr) and the approaching fluorine atom. The active space was reduced by freezing the occupancy of the lowest valence orbital. The potential is the lowest $^2A'$ surface of a three-state MRCI calculation (based on a full active space five-state SA-CASSCF) conducted with the AVTZ basis set on all atoms.

the lithium atom only) we found that the MRCI calculation required at least a three-state SA-CASSCF wave function. The calculated harpoon distance correctly follows the expected shape generated by the change in vertical ionization energy as a function of dimer length. The *ab initio* results, however, are slightly longer than predicted by simple models, which appears to be a feature of the MRCI + Q method in electron transfer systems generally.

Calculations of the lowest potentials in C_s symmetry map out the changes in the interaction potential as a function of collision geometry. The ground and $A\,^2\Sigma^+$ states become $^2A'$ states while the $B\,^2\Pi$ state becomes a $^2A'$ and $^2A''$ pair. Unfortunately, the resulting MRCI matrix for the $^2A'$ states was too large to be computed with the full valence active space. To resolve this difficulty, the lowest valence orbital outside the core was forced to be doubly occupied throughout the calculation, reducing the computational cost of the MRCI step. Extensive investigations on the effect this had on the accuracy revealed no significant changes in the potentials for the collinear and T-shaped geometries (where the reduced size of the MRCI matrix owing to the higher symmetry that could be exploited to compare results with a full active space calculation) though the outer harpoon seam moved to longer distances. This is probably a result of the reduced active space not calculating the entrance asymptotic energies to the same accuracy as before, as this harpoon seam will be very sensitive to small energy shifts at long range. The ground-state potential in Fig. 4 is based on over 800 *ab initio* geometries from a three-state MRCI calculation and shows that the outer crossing seam increases as the fluorine atom approaches from a collinear as opposed to perpendicular geometry; for example, the −10 kJ mol^{-1} energy contour changes by approximately 1.8 bohr. This shift is the result of the differences in polarization of the Li_2^+ orbital as a function of the collision angle, with the net effect that the center of positive charge moves from the center of mass toward the lithium atom closest to the fluorine.

The global energy minimum [33] occurs for the perpendicular reaction geometry, which is indicative of a charge transfer system. Furthermore, this is true for the lowest two excited $^2A'$ states (a three-state calculation includes the $^2A'$ component of the $B\,^2\Pi$ state). The $^2A'(B\,^2\Pi)$ state initially destabilizes as the reaction complex bends before strongly stabilizing at the T-shaped complex. The rapid fall in the minimum of the $2\,^2A'$ ($A\,^2\Sigma^+$) potential with bond angle does not seem to eliminate the barrier in the entrance channel. Though clearly calculations with larger basis sets need to be done to accurately access the exact energy changes involved, the results here suggest that this reaction barrier will affect all reaction geometries. Calculation for the $1\,^2B_1$ and $1\,^2B_2$ states (which form the $B\,^2\Pi$ state) for the perpendicular halogen attack suggests there is a small barrier on the $^2B_1$ surface, though its suggested height is even smaller (7.61 kJ mol^{-1}) than that on the $^2A'$ ($A\,^2\Sigma^+$) potential. The $^2B_2$ potential, which corresponds to the $^2A''$ (C_s symmetry) state, does not have a barrier, ensuring that approach along this surface is allowed at all angles at ultracold temperatures.

IV. EXIT-CHANNEL ELECTRONIC STATES

The energy changes for the $M_2 + X \rightarrow MX + M$ reactions calculated are listed in Table II. There are no experimental data for the Li_2 + F reaction and even the bond energy of LiF has yet to be measured accurately (to within 1%). We have conducted *ab initio* (MRCI + Q) calculations using a VQZ basis on lithium and an AVQZ basis on fluorine for the lowest two states of the LiF molecule and determined a D_e value of 47 991 cm^{-1} (574.1 kJ mol^{-1}), which lies within the uncertainty range of the experimental value 577 ± 21 kJ mol^{-1}. This value is also in good agreement with a recent CCSD(T) study [34] obtained at the complete basis set limit (and including relativistic and spin-orbit corrections) by Vasiliu *et al.* of 580.9 kJ mol^{-1} (with both values being clearly much higher than the full-CI result of 506.6 kJ mol^{-1} in the calculation of Bauschlicher and Langhoff [35]). Combined with the experimentally determined value [36] of D_e for Li_2 (8516.61 cm^{-1}) we calculate an

TABLE II. Calculated energy shifts for a variety of alkali-metal dimer + halogen reactions. DFT calculations were conducted with the 6-311 ++ G($3df$,$3pd$) basis set and the MPW1K functional.

Reaction	Method	Energy change (kJ mol^{-1})
Li_2 + F	DFT	−436.41
	SA-CASSCF	−383.96
	MRCI	−462.21
	Combined expt.+ theory	−472.2[a] (−477.4)[b]
Na_2 + F	DFT	−347.77
K_2 + F	DFT	−355.41
Li_2 + Cl	DFT	−344.28

[a]Result using AVQZ calculation of LiF dissociation energy (this work).

[b]Result using value calculated by Vasiliu *et al.* [34].

energy release ΔD_e of 472.2 kJ mol^{-1} for the Li_2 + F reaction, while the value based on the Vasiliu *et al.* calculation and including the spin-orbit energy of the F atom in the entrance channel is 477.4 kJ mol^{-1} (39 908 cm^{-1}). This is rather larger than the estimate from the DFT calculations but agrees reasonably well with our AVTZ three-state MRCI + Q calculation of −462.21 kJ mol^{-1}. Consequently, our calculated global minimum (AVTZ, MRCI + Q) of the ground state is −611.23 kJ mol^{-1}, while combining the best theoretical exoergicity estimate with the global minimum from Koput's CBS limit calculation of Li_2 F [27] is −625.0 kJ mol^{-1}.

From the *ab initio* value for LiF + Li($2\,^2S$) production, we can compute the reaction exoergicities of all the lithium electronic states formed in the reaction and determine what is the highest electronic state formed in this reaction at 0 K. This is complicated by the narrow separation of lithium electronic states close to the ionization limit. Furthermore, in this reaction the relatively small mass of lithium leads to a potentially significant isotope effect that must be considered. The best available frequency data for the LiF molecule comes from emission spectra recorded by Bernath and co-workers [37]: The zero-point energy in ^{7}LiF is 453.2 cm^{-1} and for ^{6}LiF it is 479.8 cm^{-1}. The corresponding energies for the Li_2 isotopes are 175.0 cm^{-1} for $^7Li_2$ [38] and 189.0 cm^{-1} in $^6Li_2$ [39]. Therefore, the energy released in the reaction has to be corrected by −278.2 cm^{-1} for ^{7}Li and −290.8 cm^{-1} in the corresponding ^{6}Li-based reaction. For both isotopes the calculated chemical energy available (using either theoretical value for the reaction exoergicity) lies between the 5g and 6s levels of the lithium atom, making the LiF + Li(5 ^2G) channel the highest energetically available with ground-state, ultracold reagents. The large isotope shift (12.6 cm^{-1} for $v = 0 \rightarrow v = 0$) will become more significant for reactions involving vibrationally excited Li_2 reagents where the opening of new closely spaced electronic channels is unavoidable.

In contrast to the situation for the entrance-channel potentials, the computed relative energies of the product asymptotes are in excellent agreement with the expected values, even when using the SA-CASSCF method. However, care must be taken now in the selection of both the basis set and the number of symmetry states included in the calculation. In Fig. 5 the lowest three SA-CASSCF $^2\Sigma^+$ states in the exit channel are presented using two different basis sets. The smaller VTZ basis set on lithium clearly fails to describe the third $^2\Sigma^+$ state correctly, an artefact corrected by using the larger AVTZ set where the state in question approaches the correct asymptotic limit.

Figure 6 presents the lowest four $^2\Sigma^+$ and two $^2\Pi$ states in the exit channel calculated by Balint-Kurti (panel a) using the OM method and the corresponding states calculated here (panel b) using the SA-CASSCF method. It is immediately apparent that the earlier calculation has a long-range minimum in the first excited $^2\Sigma^+$ state corresponding to an ionic surface that is not seen in the present four-state SA-CASSCF results. However, inspection of the wave functions in Fig. 6(b) reveals that all the states are in fact of mixed covalent-ionic character, the ionic component present in the rising side of the potential curves. The $^2\Pi$ states presented were found using a two-state SA-CASSCF calculation and are both repulsive. The calculated energy of the Li($2p$) and Li($3s$) asymptotes are 14 830 and 26 887 cm^{-1} and compare well

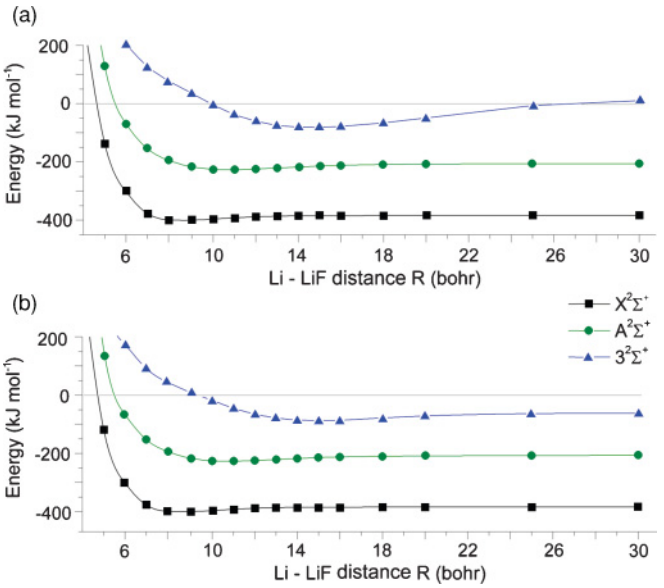

FIG. 5. (Color online) The Li_2 + F exit-channel potentials for the lowest three $^2\Sigma^+$ states calculated (a) at the SA-CASSCF level with the VTZ(Li) and AVTZ(F) basis sets and (b) with the basis set on lithium now AVTZ as well.

with the experimental values of 14 903 and 27 205 cm^{-1} (Table III). In Fig. 5, the VTZ calculation clearly fails to get the correct dissociation energy for the third state but highlights the ionic state that effectively slices through a series of repulsive covalent $^2\Sigma^+$ states to form nested bound electronic states.

An understanding of the nature of this ionic state requires consideration of the possible ionic products that can be formed.

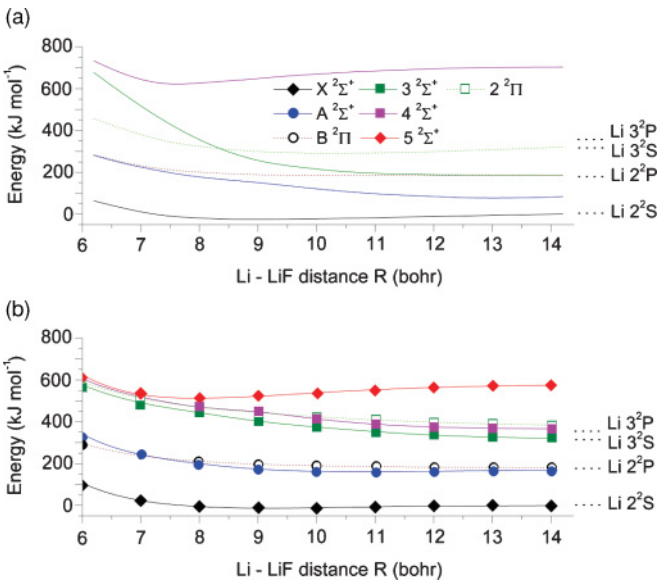

FIG. 6. (Color online) Li_2 + F exit-channel potentials for the lowest $^2\Sigma^+$ (solid lines) and $^2\Pi$ (dashed lines) states calculated (a) with the OM method by Balint-Kurti [15] and (b) at the SA-CASSCF level with the AVTZ(Li) and AVTZ(F) basis sets. In (a) the asymptotic limits are taken from experiment while in (b) the limits are those calculated in this study and tabulated.

TABLE III. Li_2 + F reaction exit channels and molecular symmetries. The relative energies are the experimental values for the electronic states of the lithium atom.

Li fragment state	Molecular states	Relative energy (cm^{-1})	SA-CASSCF (cm^{-1})	MRCI + Q (cm^{-1})
2^2S	$^2\Sigma^+$	0	0	0
2^2P	$^2\Sigma^+$,$^2\Pi$	14 903	14 830	14 843
3^2S	$^2\Sigma^+$	27 205	26 887	27 100
3^2P	$^2\Sigma^+$,$^2\Pi$	30 925	30 582	–

The electron affinity of LiF has not been accurately determined by experiment with the one quoted measurement [40] just placing a lower limit of 1.35 eV. This would make it one of the highest electron affinities of the alkali-metal halides and would be at odds with the trend in electron affinity (EA) observed by Miller *et al.* [41]. These authors suggest the following formula to estimate the electron affinity for the alkali-metal halides:

$$\mathrm{EA} = 1.189 - \frac{0.103\alpha_M}{r_{MX}^2},$$

where α_M is the alkali-metal polarizability (20.63 $Å^3$) and r_{MX} is the equilibrium bond distance of the neutral alkali-metal halide molecule (1.563 Å for LiF [42]). The resulting EA estimate for LiF is just 0.3193 eV, by far the smallest value of all the alkali-metal halides. Note that Miller *et al.* warn that their formula is robust for values of $\frac{\alpha_M}{r_{MX}^2} \sim 3$–7 Å whereas this value is ~8.445 Å for LiF; however, this value is in good agreement with *ab initio* calculations of 0.356 eV [43] [CCSD(T)] and 0.35 eV [44] [QCISD(T)] and will be adopted here as a feasible lower limit. Yet, despite the relatively small electron affinity of LiF, the low ionization energy of Li ensures that only 40 910 cm^{-1} of energy is required to produce the $LiF^- + Li^+$ ionic products relative to ground-state neutrals. This upper limit strongly suggests that the formation of charged products lies within 1000 cm^{-1} of the zero-energy exoergicity.

In Fig. 7(a) four-state MRCI + Q potentials are presented for the exit channel as broadly agreeing with the corresponding SA-CASSCF potentials though the potential well in the $3\,^2\Sigma^+$ state at $\theta_{\mathrm{exit}} = 180^\circ$ has clearly deepened significantly (with well depth now being 1760 cm^{-1}). This well is the result of a pair of avoided crossings between the ionic and covalent surfaces. Comparison with the $\theta_{\mathrm{exit}} = 0^\circ$ geometry in Fig. 7(b) reveals the greater stability of the ionic potential when the halogen is between the two lithium species, with the broad features of the MXM ground state very reminiscent of the equilibrium geometry ($\theta_{\mathrm{exit}} = 66^\circ$; for example, the ground-state well depth is similar at both bond angles). To facilitate comparison between the two calculations, the four-state SA-CASSCF results in Fig. 7(b) are corrected to compensate for the significant underestimation of the chemical exoergicity by shifting the Li($2\,^2S$) asymptote to match the four-state MRCI + Q result (based itself on a SA-CASSCF wave function) in Table I. Note that the relative SA-CASSCF energies of the exit-channel asymptotes are in very close agreement with the MRCI + Q results. Clearly illustrated are the multiple crossings between the ionic surface and the covalent exit potentials. Furthermore, there is obviously an additional ionic potential that forms the true minima of the $3\,^2\Sigma^+$ state. This must correspond to an excited Σ^+ state of the LiF^- anion because the Li^+ cation has no valence electrons.

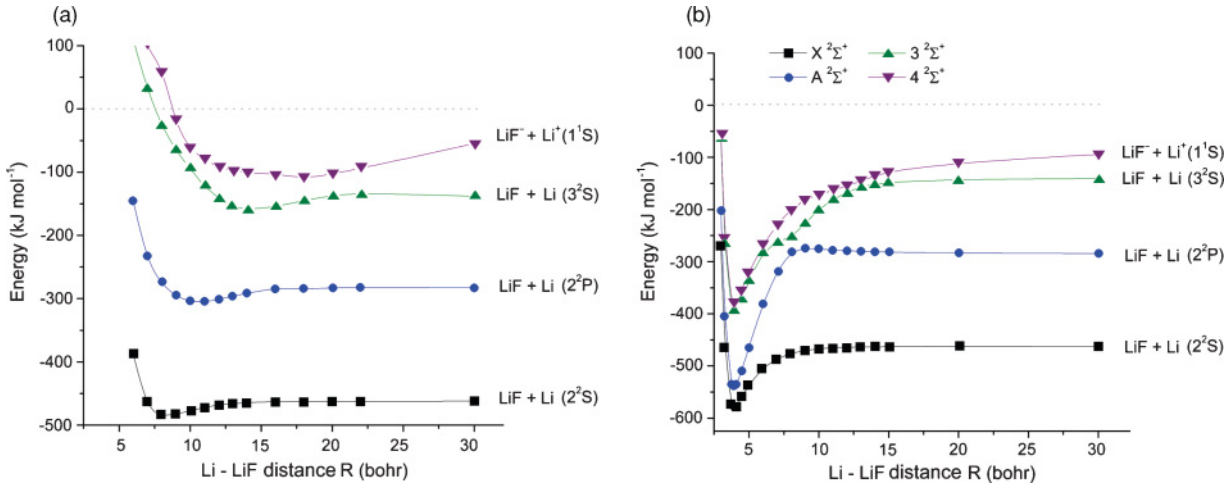

FIG. 7. (Color online) (a) Li_2 + F exit-channel potentials for the lowest four $^2\Sigma^+$ states calculated at the MRCI + Q level with the AVTZ(Li) and AVTZ(F) basis sets for the geometry corresponding to a collinear MMX reaction complex ($\theta_{\mathrm{exit}} = 180^\circ$). (b) Exit-channel potentials corresponding to MXM ($\theta_{\mathrm{exit}} = 0^\circ$) for the lowest four $^2\Sigma^+$ states calculated at the SA-CASSCF level with the AVTZ(Li) and AVTZ(F) basis sets. All LiF products are in the $^1\Sigma^+$ state and the LiF^- anion is in its ground $^2\Sigma^+$ state. Zero energy (gray dashed line) corresponds to the Li_2 minimum in the entrance channel. The energy of the SA-CASSCF asymptote for the Li($2\,^2S$) exit channel has been shifted to match the MRCI + Q calculation in panel (a); see text for further details.

The minimum of the ground state of the Li_2F complex is clearly ionic and appears to be of the form $Li_2{}^+F^-$ but what subsequently takes place upon release of the lithium fragment in the exit channel is sensitive to the geometric arrangement of the three atoms and the electronic state of the lithium atom product. In the collinear collision complex, the released lithium is separated from the fluorine atom by the second lithium atom and as the fragment moves further away on the lowest potentials the positive charge remains firmly on the intermediate lithium atom. Thus the interaction potential is essentially a covalent one between the departing lithium neutral atom and the polar (and ionic) LiF molecule. However, if the complex is at the equilibrium geometry and the lithium departs, the positive charge is still spread over the lithium dimer and the leaving group appears to be trying to overcome the Coulomb force between $Li_2{}^+$ and F^-. Consequently, the energy required to form the lithium atom product is greater than the dissociation energy of an isolated $Li_2{}^+$ cation. The result is that the production of ground-state Li($2s$) and ($2p$) products will proceed by subtly different mechanisms depending on the exit angle adopted by the products: A collinear reaction will be nonionic whereas one at the equilibrium geometry takes place along the ionic surface. The Li($3s$) products (and all atomic states higher in energy) will involve the ionic reaction pathway at all angles.

V. FESHBACH MOLECULES AND THE $LI_2 + F$ REACTION

The possibility of studying ultracold chemical reactions, where all reagents are thermalized at ultracold temperature, has captured the imagination of many working in the cold atom field. There is compelling evidence that ultracold atom-diatomic exchange reactions have already been observed between K or Rb atoms and KRb molecules and even a bimolecular reaction between ultracold fermionic KRb heteronuclear dimers. Reactions between alkali-metal dimers and alkali-metal atoms are barrierless reactions and are consequently rapid at very low temperatures. However, these reactions involved tiny releases of chemical energy. Studying reactions with ultracold molecules offers the possibility of unprecedented control over the internal and kinetic energies present within a reaction. Unfortunately, at present there is no simple method to cool molecules from room temperature down to the ultracold temperature regime.

The $H_2 + F$ reaction is a benchmark in theoretical dynamics due to the presence of just one nonhydrogenic atom and the small number of electrons (11) present. In addition, there is now a wealth of experimental data to test the accuracy of the best *ab initio* surfaces. It is natural, therefore, that $H_2 + F$ has also been studied as a candidate for ultracold chemistry [45] as well. However, the reaction has a considerable barrier in the entrance channel and at present there is no known way to cool hydrogen molecules or indeed hydrogen atoms into the ultracold regime. By contrast, Li_2 molecules at ultracold temperatures have already been prepared in the laboratory. In addition, the calculations here demonstrate that the $Li_2 + F$ reaction has no barrier. Both reactions are further influenced by spin-orbit coupling which is present in the ground state of the fluorine atom. The four-fold degenerate $^2P_{3/2}$ ground fine-structure state of the fluorine atom correlates to the $^2\Sigma^+$ state and the $^2\Pi_{3/2}$ components of the $^2\Pi$ state, while the doubly degenerate $^2P_{1/2}$ become the $^2\Pi_{1/2}$ components. One effect of the spin-orbit splitting is that the covalent state forming the long-range part of the ground state will be $\sim$100 cm^{-1} lower in energy, and therefore the crossing distance will be shorter than calculated in its absence. This would not affect the barrierless nature of the interaction in $Li_2 + F$.

It is worth considering how the lack of collision energy in an ultracold reaction will affect the dynamics of the $Li_2 + F$ reaction at ultracold temperatures. The long-range nature of the initial ionic-covalent crossing seems to preclude its participation in the entrance-channel dynamics because of the small surface coupling expected. However, Stearn and Eyring [46] have shown that the probability of crossing should have a $T^{-1/2}$ dependence, which clearly favors participation at lower temperatures. Thermal reactions involve all three lowest states, but the tiny velocities of the reagents at ultracold temperatures will have a dramatic effect on the significance of each individual state in the reaction. At room temperature, the $1\,^2\Pi$ state dominates the reaction because it is doubly degenerate. However, the potential well of this state is formed by the $1\,^2\Pi_u$ state of the $Li_2{}^+$ ion: This state can radiate to ground-state $Li_2{}^+(1\,^2\Sigma_g^+)$. The lifetime of the corresponding $1\,^2\Pi_u$ state in $Na_2{}^+$ is calculated [47] to be of the order of 11–12 ns and a simple estimate can be made on the effect of radiative decay on the reaction pathway: If one assumes that the $1\,^2\Pi$ state will radiate to ground only while inside the potential well, and since there are very strong repulsive forces in the exit channel then this must take place in the entrance channel. The window for decay is therefore $\sim$ 1 Å and in order for decay to take place this must take more than $\sim$10 ns to cover. A collisional velocity of 0.01 m s^{-1} is therefore required, or a temperature below 100 nK. At such temperatures, all the nuclear flux will follow the $X\,^2\Sigma^+$ potential into the exit channel. Of course, we have ignored the strong acceleration that will also take place in the entrance channel once the potential well is reached, but clearly the $X\,^2\Sigma^+$ state will play a more significant role at ultracold temperatures than in thermal reactions, with or without a barrier on the $1\,^2\Pi$ surface.

The biggest experimental hurdle to studying the reactions between alkali-metal dimers and halogen atoms are the difficulties in producing ultracold halogens. No optical cooling pathway is yet known. Fortunately, halogens are paramagnetic atoms and can in principle be decelerated using the multistage atom coilgun developed by Raizen and co-workers [48] and then sympathetically cooled to the ultracold regime. However, even in the absence of a source of ultracold halogen atoms, ultracold technology offers an opportunity to study these reactions at the state-to-state level using the unique properties of ultracold alkali-metal metal dimers formed within clouds of an ultracold gas: By using magnetic tuning of Feshbach (quantum) scattering resonances [49], ultracold atoms are efficiently converted into molecules and molecular BEC states have been formed in the likes of Li_2 [50], K_2 [51], and Rb_2 [52]. The resulting dimers possess almost no kinetic energy and just a single rovibronic energy state, yet since this energy state is close to the dissociation limit the internal energy of the molecules formed is extremely high and the radial wave functions are highly asymmetrical and concentrated around

the outer turning point R_{out}. By releasing halogen atoms into a cloud of trapped ultracold Li, the hot atoms will initially participate in elastic and inelastic collisions with the ultracold atoms. However, on application of the magnetic field the dimers are formed and now reactive collisions are possible.

Feshbach resonances are known as quantum halo states [53] and can be characterized [54] as "open" or "closed" resonances, the latter possessing a strong molecular component. Although they have a significant open-channel ("atomic pair") component, it is only the closed-channel ("molecular") component that will be involved in any atom-diatomic reactive collisions. By tuning the magnetic field a variety of molecular Feshbach resonances can be accessed associated with a range of radial wave functions ("vibrational levels"). In addition, it is possible to select Feshbach resonances with $\ell = 0$, 2, 4, etc. (where ℓ is the orbital angular momentum of the paired alkali-metal atoms) and therefore control the "rotational wave function" of the molecules as well: For example, a *g*-wave shape resonance has been produced [55] in ^{85}Rb. Unlike the traditional molecular beam methods, a single quantum state is created by the magnetic field and in particular a nonzero angular momentum state can be selectively populated; this angular momentum state control is a significant advantage of Feshbach prepared molecules. The individual Feshbach resonances have a wide range of linewidths (measured in terms of the magnetic field) and couplings with the environment. This suggests that although only a small energy may separate two resonances, their reactive properties should be very different and strongly affect the product branching ratios.

The unique features of the harpoon reaction studied in this paper could be exploited fully by the single quantum state preparation that is possible in Feshbach molecules. The present calculations support the harpoon model involving electron transfer from the Li_2 molecule to the incoming fluorine atom, and the resulting Li_2^+ and F^- pair attract one another along the corresponding ionic potential until the bonding is rearranged and the exit dynamics is again dominated by a transfer between surfaces, from the ionic back to the covalent. This process is the (microscopic) reverse of the quenching mechanism [56] observed in the deactivation of electronic excited alkali-metal atoms by molecules. From a study of the PE surfaces [57] the exit-channel transfer from ionic to covalent should take place at the appropriate harpoon radius for each LiF + Li(nL) channel (Table IV) where the ionic-covalent coupling is at a maximum. The crossing point between the ionic potential and the covalent potentials can be estimated in the harpoon model from the simple formula (with polarization effects ignored)

$$R = \frac{Z^2}{4\pi\varepsilon_0 \Delta E} = \frac{14.399\,647}{\Delta E\ (\mathrm{eV})}\mathring{A}.$$

Here ΔE is the difference between the electronic energy of the Li atom product and the ionic asymptote energy, determined from the electron affinity of the LiF and the accurately known ionization energy of the lithium atom (the value 40 910 cm^{-1} derived earlier is used here). The results are tabulated in Table IV and it is clear that the simple calculation matches closely the barrier top on the A state calculated by MRCI [Fig. 7(b)]. The excited-state crossings are somewhat more extended than the SA-CASSCF calculations suggest but this is the result of the tendency for state-averaged CASSCF calculations to underestimate the harpoon radii at extended bond lengths (as observed in the entrance channel).

TABLE IV. Estimated crossing radii for the exit channels of the Li_2 + F reaction. The energy separation is calculated using the LiF electron affinity and the energy states of lithium [58] and is relative to the ionic asymptote. The value in brackets in the top row is the *ab initio* location for the top of the barrier in the A state for the D_{2h} geometry. The emission wavelengths correspond to a transition terminating on the 2*s* state of lithium.

Li final state	Energy) (cm^{-1})	Emission line (nm)	Exit harpoon radius (Å)
2*p*	−26 007	671	4.47(4.39)
3*s*	−13 705	821[a]	8.47
3*p*	−9985	323	11.63
4*p*	−4441	274	26.15
5*p*	−1895	256	61.29
6*p*	−520	248	223.36

[a]Emission terminates at the 2*p* state.

These longer harpoon radii are of comparable size to molecular quantum states close to the dissociation limit (Fig. 8). By tuning the magnetic field, different resonances of the dimers are accessed with a different Li-Li separations (R_{out}) and those product channels with a harpoon radius of comparable bond length ought to cross efficiently between surfaces. Those exit channels with a significantly different harpoon radius to the Feshbach length, however, should be effectively closed, facilitating control over the production of specific Li quantum states by selection of a particular Feshbach resonance. Thus control over the branching ratio is achieved. Multiple ionic-neutral crossings should also be present in the all alkali-metal exchange reactions too but here the lack of chemical exoergicity means that long-range ground-state reagents cannot access the crossing regions of the excited electronic state products at ultracold collision energies. Reactions, however, involving excited electronic states of the alkali dimers with a third alkali-metal atom would have sufficient energy to access this long-range region. It is worth noting that significant population inversions in the electronic states of Cs have been reported [59] in a high-temperature Cs-Cl reaction chamber where the Cs_2 + Cl reaction is believed to be a significant contributor. As the highest bound vibrational state changes across the dimers $^6Li_2$ ($v = 38$), $^6Li^7Li$ ($v = 39$), and $^7Li_2$ ($v = 41$), isotope effects are also expected to be significant [60]. Finally, the vibrational energy of the Feshbach molecules is sufficient to create the ionic products LiF^- and Li^+.

Unlike rival attempts to control a reaction through vibrational excitation, Feshbach molecules have a number of unique advantages: (1) The sensitivity of the bond length to the selected quantum state is much larger close to the dissociation limit than at lower vibrational energies [for example, using a Li_2 Casimir-Polder potential [61], R_{out} changes from ∼105 Å at −140 kHz to ∼159 Å at −12 kHz (with the level measured relative to the dissociation limit)]; (2) the radial wave functions have a high asymmetry [62] as they lie close to the dissociation limit, unlike lower vibrational levels where the potential is more harmonic with symmetrical wave functions: (3) the

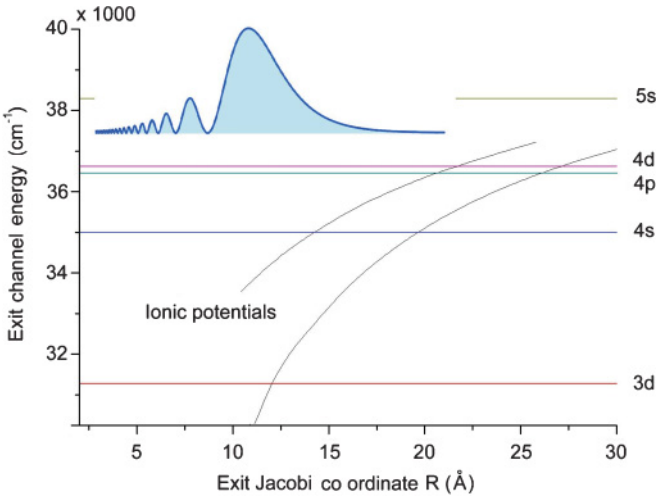

FIG. 8. (Color online) (a) Schematic Li_2 + F long-range exit-channel crossing between the ionic and covalent potentials for the product channels producing lithium atoms in the $3d$ to $5s$ electronic states. Also shown is Ψ^2 for the $v = 40$ vibrational level of $^7Li_2$ [62] on the same length scale. The $v = 40$, $J = 6$ level lies just 0.026 cm^{-1} from the $^7Li_2$ dissociation limit.

energy separation between quantum states is tiny close to dissociation so that any change in the dynamics is due to changes in the radial molecular wave function and not the vibrational energy.

VI. CONCLUSION

In this paper, potentials have been presented to support the simple harpoon model of reactions in the Li_2 + F molecular system. The entrance channel consists of at least two ionic-covalent crossing regions, the outer one accessible at all collision angles while the inner one appears to possess a barrier in the collinear approach. A number of features of the surfaces involved have been clarified:

(1) Both the $X\,^2A'$ and $1\,^2A''$ states allow barrierless reactions that are accessible to ultracold reagents at all geometries. There is a significant increase in the long-range harpoon distance (~0.9 Å) in the $X\,^2A'$ state as the geometry changes from T-shaped to collinear, reflecting the change in polarization of the Li_2^+ ($1\,^2\Sigma_g^+$) dimer as a function of angle.

(2) The $^2A'$ ($A\,^2\Sigma^+$) state appears to have an energy barrier at all geometries. Its height (~20 kJ mol^{-1}) is greater than the zero-point energy of the Li_2 reagents. A barrier also exists on the $^2A'$ ($B\,^2\Pi$) surface but it is less than half the size of the one on the $^2A'$ ($A\,^2\Sigma^+$) surface. The exact heights of these barriers are sensitive to the basis set used and should be investigated more thoroughly. All three of the lowest $^2A'$ states have a T-shaped global minimum indicative of an ionic complex.

(3) The exit-channel potentials are characterized by a series of long-range avoided crossings between the covalent potentials correlating to the excited electronic states of the lithium atom products and an ionic $^2A'$ surface leading to the products LiF^- ($X\,^2\Sigma^+$) + $Li^+(^1S)$. Even with ultracold reagents and zero-point energy alone chemiluminescent excited states up to the Li($5\,^2G$) state should be detected. The calculations identify a strong geometry dependence in the ionic potentials and two fragmentation mechanisms for the $Li_2{}^+F^-$ complex. All the calculated surfaces have deeply bound potential wells in the LiFLi geometry, while those of $^2\Pi$ symmetry are repulsive in the alternative LiLiF collinear complex. The results also reveal a number of electronically excited states of the LiF^- anion.

All the possible alkali-metal dimers (hetero- and homonuclear) and halogen atom combinations react to form electronically excited alkali-metal products, though the exoergicity of the reaction studied in this paper is the largest. Calculating all the relevant surfaces involved, even for a collision with ultracold reagents, would be a considerable challenge because of the large number of product states that can be formed. However, the simple description of the dynamical interaction within the harpoon framework suggests it may be possible to produce highly accurate surfaces by a combination of *ab initio* and analytical descriptions of the potentials, particularly at long range.

ACKNOWLEDGMENTS

The authors would like to thank Ruiping Chen and Daniel Rogers for help with the initial *ab initio* calculations and Patryk Jasik for sending preliminary data on the Li_2^+ cation. KWAW thanks UK Department for Employment and Learning (DEL) for funding.

[1] W. D. Phillips and H. Metcalf, Phys. Rev. Lett. **48**, 596 (1982).
[2] M. H. Anderson, J. R. Ensher, M. R. Matthews, C. E. Wieman, and E. A. Cornell, Science **269**, 198 (1995).
[3] P. S. Julienne, Faraday Discuss. **142**, 361 (2009).
[4] S. Ospelkaus, K.-K. Ni, M. H. G. de Miranda, B. Neyenhuis, D. Wang, S. Kotochigova, P. S. Julienne, D. S. Jin, and J. Ye, Faraday Discuss. **142**, 351 (2009).
[5] T. Köhler, K. Góral, and P. S. Julienne, Rev. Mod. Phys. **78**, 1311 (2006).
[6] P. Davidovits and D. L. McFadden, *Alkali Halide Vapors*, (Academic, New York, 1979).
[7] F. Haber and W. Zisch, Z. Phys. **9**, 302 (1922); M. Polanyi and G. Schay, Z. Phys. Chem B **1**, 30 (1928).
[8] W. S. Struve, J. R. Krenos, D. L. McFadden, and D. R. Herschbach, J. Chem. Phys. **62**, 404 (1975).
[9] J. L. Magee, J. Chem. Phys. **8**, 687 (1940).
[10] E. S. Rittner, J. Chem. Phys. **19**, 1030 (1951).
[11] S. Knoop, F. Ferlaino, M. Berninger, M. Mark, H.-C. Nägerl, R. Grimm, J. P. D'Incao, and B. D. Esry, Phys. Rev. Lett. **104**, 053201 (2010).
[12] S. Ospelkaus, K.-K. Ni, D. Wang, M. H. G. de Miranda, B. Neyenhuis, G. Quéméner, P. S. Julienne, J. L. Bohn, D. S. Jin, and J. Ye, Science **327**, 853 (2010).

[13] D. Sengupta and A. K. Chandra, J. Mol. Struct. **492**, 29 (1999).
[14] For a comprehensive list of chemiluminescence studies of harpoon reactions up to 1977 consult D. L. McFadden, Chemiluminescence in Gas Phase Alkali Halide Systems, in *Alkali Halide Vapors* (Academic, New York, 1979).
[15] G. G. Balint-Kurti, Ph.D. thesis, Harvard University, 1969.
[16] P. Siegbahn and H. F. Schaefer III, J. Chem. Phys. **62**, 3488 (1975).
[17] B. A. Bushaw, W. Nörtershäuser, G. W. F. Drake, and H. J. Kluge, Phys. Rev. A **75**, 052503 (2007).
[18] A. L. Roche and Ch. Jungen, J. Chem. Phys. **98**, 3637 (1993).
[19] C. Blondel, C. Delsart, and F. Goldfarb, J. Phys. B **34**, L281 (2001).
[20] S. Mangier and M. Aubert-Frecon, J. Quant. Spectrosc. Radiat. Transfer **75**, 121 (2002).
[21] D. M. Bishop and C. Pouchan, J. Chem. Phys. **80**, 789 (1984).
[22] K. Andersson, P. A. Malmqvist, and B. O. Roos, J. Chem. Phys. **96**, 1218 (1992).
[23] T. H. Dunning Jr., J. Chem. Phys. **90**, 1007 (1989).
[24] A. J. C. Varandas, J. Chem. Phys. **131**, 124128 (2009).
[25] S. R. Langhoff and E. R. Davidson, Int. J. Quantum Chem. **8**, 61 (1974).
[26] B. J. Lynch, P. L. Fast, M. Harris, and D. G. Truhlar, J. Phys. Chem. A **104**, 4811 (2000).
[27] A. Granovsky, FIREFLY version 7.0, [http://classic.chem.msu.su/gran/gamess/index.html].
[28] J. Koput, J. Chem. Phys. **129**, 154306 (2008).
[29] P. Jasik and J. E. Sienkiewicz, Chem. Phys. **323**, 563 (2006).
[30] P. Jasik (private communication).
[31] A. W. Jasper, M. D. Hack, D. G. Truhlar, and P. Piecuch, J. Chem. Phys. **116**, 8353 (2002).
[32] H. Bouzouita, C. Ghanmi, and H. Berricke, J. Mol. Struct. **777**, 75 (2006).
[33] K. W. A. Wright, D. E. Rogers, and I. C. Lane, J. Chem. Phys. **131**, 104306 (2009).
[34] M. Vasiliu, S. Li, K. A. Peterson, D. Feller, J. L. Gole, and D. A. Dixon, J. Chem. Phys. Chem. A **114**, 4272 (2010).
[35] C. W. Bauschlicher Jr. and S. R. Langhoff, J. Chem. Phys. **89**, 4246 (1988).
[36] W. T. Zemke, W. C. Stwalley, J. Phys. Chem. **97**, 2053 (1993).
[37] H. G. Hedderich, I. Frum, R. Engleman Jr., and P. F. Bernath, Can. J. Chem. **69**, 1659 (1991).
[38] E. Sangfeit, H. A. Kurtz, N. Elande, and O. Goscinski, J. Chem. Phys. **81**, 3976 (1984).
[39] X. Wang, J. Yang, J. Qi, and A. M. Lyyra, J. Mol. Spectrosc. **191**, 295 (1998).
[40] H. Z. Ebinghaus, Z. Naturfor. **19a**, 727 (1964).
[41] T. M. Miller, D. G. Leopold, K. K. Murray, and W. C. Lineberger, J. Chem. Phys. **85**, 2368 (1986).
[42] L. Wharton, W. Klemperer, L. P. Gold, R. Strauch, J. J. Gallagher, and V. E. Derr, J. Chem. Phys. **38**, 1203 (1963).
[43] G. L. Gutsev, M. Nooijen, and R. J. Bartlett, Chem. Phys. Lett. **276**, 13 (1997).
[44] A. I. Boldyrev, J. Simons, and P. von R. Schleyer, J. Chem. Phys. **99**, 8793 (1993).
[45] N. Balakrishnan and A. Dalgarno, Chem. Phys. Lett. **341**, 652 (2001).
[46] A. E. Stearn and H. Eyring, J. Chem. Phys. **3**, 778 (1935).
[47] S. Magnier and F. Masnou-Seeuws, Mol. Phys. **89**, 711 (1996).
[48] E. Narevicius, C. G. Parthey, A. Libson, J. Narevicius, I. Chavez, U. Even, and M. G. Raizen, New J. Phys. **9**, 358 (2007).
[49] E. Tiesinga, B. J. Verhaar, and H. T. C. Stoof, Phys. Rev. A **47**, 4114 (1993).
[50] S. Jochim, M. Bartenstein, A. Altmeyer, G. Hendl, S. Riedl, C. Chin, J. Hecker Denschlag, and R. Grimm, Science **302**, 2101 (2003).
[51] C. A. Regal, C. Ticknor, J. L. Bohn, and D. S. Jin, Nature (London) **424**, 47 (2003).
[52] S. Dűrr, T. Volz, A. Marte, and G. Rempe, Phys. Rev. Lett. **92**, 020406 (2004).
[53] A. S. Jensen, K. Riisager, D. V. Fedorov, and E. Garrido, Rev. Mod. Phys. **76**, 215 (2004).
[54] P. S. Julienne and B. Gao, AIP Conf. Proc. **869**, 181 (2006).
[55] H. M. J. M. Boesten, C. C. Tsai, B. J. Verhaar, and D. J. Heinzen, Phys. Rev. Lett. **77**, 5194 (1996).
[56] K. J. Laidler, J. Chem. Phys. **10**, 34 (1942).
[57] W. S. Struve, Mol. Phys. **25**, 777 (1973).
[58] L. J. Radziemski, R. Engleman Jr., and J. W. Brault, Phys. Rev. A **52**, 4462 (1995).
[59] L. H. Hall, Appl. Phys. Lett. **27**, 335 (1975).
[60] R. J. le Roy, N. S. Dattani, J. A. Coxon, A. J. Ross, P. Crozet, and C. Linton,, J. Chem. Phys. **131**, 204309 (2009).
[61] M. Marinescu and L. You, Phys. Rev. A **59**, 1936 (1999); A. Salam, *ibid.* **62**, 026701 (2000).
[62] J. A. Coxon and T. C. Melville, J. Mol. Spectrosc. **235**, 235 (2006).